DOI: 10.1002/ejic.201100200

Magnetism in Giant Unit Cells – Crystal Structure and Magnetic Properties of $R_{117}Co_{52+\delta}Sn_{112+\gamma}$ (R = Sm, Tb, Dy)

Kirill Kovnir[a] and Michael Shatruk*[a]

Dedicated to Professor John D. Corbett on the occasion of his 85th birthday

Keywords: Intermetallic phases / Polyhedra / Rare earths / Magnetic properties

Ternary polar intermetallics $Sm_{117}Co_{55.6}Sn_{116}$, $Tb_{117}Co_{59}Sn_{111}$, and $Dy_{117}Co_{58}Sn_{111}$ were prepared by the arc-melting technique. They belong to the $Tb_{117}Fe_{52}Ge_{112}$ structure type and are characterized by a giant cubic unit cell ($V >$ 25000 Å^3). The build-up of the structure can be understood by identifying three basic metal-centered polyhedra, a 14-vertex $Co@Co_6Sn_8$ at the edge centers and at the body center of the unit cell, a 14-vertex $Sm@Co_8Sn_6$ at the origin of the unit cell, and a 22-vertex $Sm@Co_{12}Sn_{10}$ at the center of each octant. The rest of the atoms in the crystal structure can be considered as forming concentric polyhedra around these basic units. Such an approach results in three types of large multishell polyhedra that share their outermost faces and provide complete space filling. The arrangement of these polyhedra follows the arrangement of atoms in the structure of Heusler alloy Cu_2MnAl. The description of this complex structure in terms of multishell clusters allows its separation into regions of different polarity, as each individual shell is composed of either Sm or Co/Sn atoms. $Sm_{117}Co_{55.6}Sn_{116}$ exhibits ferromagnetic ordering in the Sm sublattice at 86 K. $Tb_{117}Co_{59}Sn_{111}$ and $Dy_{117}Co_{58}Sn_{111}$ undergo consecutive paramagnet–ferromagnet and ferromagnet-canted–antiferromagnet phase transitions when the temperature is lowered. The transitions take place at 38 K and 20 K for $Tb_{117}Co_{59}Sn_{111}$ and at 30 K and 11 K for $Dy_{117}Co_{58}Sn_{111}$.

Introduction

Intermetallics represent one of the most structurally diverse classes of chemical compounds. In contrast to organic matter, where the myriad of structures and compositions is essentially due to the prolific ability of one element (carbon) to form homonuclear bonds, the abundance of intermetallic compounds stems from the great variety of constituent elements and coordination environments. The structural complexity that can be generated by these two factors is astonishing, while the aesthetic beauty of these often highly symmetric structures is truly fascinating.

Samson was the first one to note that an intricately disordered crystal structure with more than a thousand atoms in the unit cell hid behind a deceitfully simple composition of $NaCd_2$. Indeed, both Samson and later Andersson et al. showed that the actual composition is approximately $Na_{1.1}Cd_{1.9}$.[1] Similarly complex structures were later found for binary compounds Mg_2Al_3,[2] $Sm_{11}Cd_{45}$,[3] Cd_3Cu_4,[4] $K_{17}In_{41}$,[5] and γ-brasses (e.g. $Cu_{41}Sn_{11}$[6]). Ternary phases exhibit even more complicated structures, with $Al_{55.4}Cu_{5.4}Ta_{39.1}$ having the largest unit cell reported to date.[7] The current interest in such phases is motivated by their possible application as thermoelectrics, hydrogen storage materials, heterogeneous catalysts, or as models for understanding complex nanoscale architectures.[8,9]

Various approaches have been proposed to comprehend these complicated crystal structures. The original ideas of Samson, who defined the structure of $NaCd_2$ in terms of interconnected Friauf polyhedra,[1] were extended by Parthé, who introduced a concept of nested polyhedral units related to fragments found in the simplest structure types.[10] These concepts originated from early ideas of Bradley and Jones, who represented complexes structures as an assembly of concentric polyhedra.[11] This approach is also useful for describing structures of quasicrystals and their approximants, as was shown by Corbett.[12] Frank and Kasper considered complex intermetallics as a tetrahedral close packing of spheres.[13] Recently, Lee and Hoffmann have rationalized a number of such structures as emerging from interpenetrating polar and nonpolar sublattices.[14]

Among all these efforts to understand and properly explain the structures of intermetallics with giant unit cells (> 20000 Å^3, Table 1), phases of general composition $R_{117}M_{52+\delta}X_{112}$ (R = rare-earth metal, M = 3d transition metal, X = Ge, Sn) remain surprisingly overlooked. A series

[a] Department of Chemistry and Biochemistry, Florida State University,
95 Chieftan Way, Tallahassee, FL 32306-4390, USA
Fax: +1-850-644-8281
E-mail: shatruk@chem.fsu.edu

Supporting information for this article is available on the WWW under http://dx.doi.org/10.1002/ejic.201100200.

of germanides ($\delta = 0$) was reported by Pecharsky et al. in the 1990s,[17] and two Sn analogues ($\delta = 5$) with R = Dy[19] and Pr[20] were described afterwards. Nevertheless, a detailed analysis of the crystal structure build-up is missing, and nothing beyond the structural characterization is known about these phases, except for a brief mention of magnetic properties of $Pr_{117}Co_{57}Sn_{112}$. The large concentration of the rare-earth metal (ca. 40 atom-%) suggests that such phases can exhibit interesting magnetic behavior with potentially high magnetic ordering temperatures. Furthermore, the complexity of the structure might result in the interesting influence of the short-range structural disorder on the long-range magnetic ordering (such as emergence of spin-glass behavior).

Table 1. Intermetallic compounds with giant unit cells.

Compound	Volume /Å^3	Space group	Ref.
$Li_{13}Na_{29}Ba_{19}$	20424	$F4\bar{3}m$	[15]
$K_{51}Sn_{82}$	20834	$P2_1/c$	[16]
Mg_2Al_3	22518	$Fd\bar{3}m$	[2]
$Tb_{117}Fe_{52}Ge_{112}$	23345	$Fm\bar{3}m$	[17]
$Gd_{117}Fe_{52}Ge_{112}$	23808	$Fm\bar{3}m$	[18]
$Cs_{52}Sn_{82}$	24472	$P2_1/c$	[16]
$Dy_{117}Co_{57}Sn_{112}$	26546	$Fm\bar{3}m$	[19]
$NaCd_2$	28540	$Fd\bar{3}m$	[1]
$Pr_{117}Co_{57}Sn_{112}$	29276	$Fm\bar{3}m$	[20]
$CaCd_{1.58}Au_{0.42}$	30522	$I4_1/amd$	[21]
$Li_{33.3}Ca_{2.96}Ba_{13.08}$	30978	$R\bar{3}c$	[22]
$Li_{8.9}Na_{8.3}Ba_{15.3}$	33552	$P\bar{3}$	[22]
$Li_{0.87}Zn_{0.98}Ga_{1.93}$	42388	$P6mmm$	[23]
$Al_{56.6}Cu_{3.9}Ta_{39.5}$	93428	$F4\bar{3}m$	[7]
$Al_{55.4}Cu_{5.4}Ta_{39.1}$	365372	$F4\bar{3}m$	[7]

Herein, we demonstrate how one can make sense of these $Tb_{117}Fe_{52}Ge_{112}$-type structures by analyzing them in terms of nested (concentric) polyhedra. We report the preparation and detailed structural analysis of $R_{117}Co_{52+\delta}Sn_{112+\gamma}$ (R = Sm, Tb, Dy), elaborating the reasons for the varying stoichiometry of these compounds and dissecting their structural organization. Magnetic properties of these materials are also discussed.

Results and Discussion

Synthesis

Initially, we obtained single crystals of $Sm_{117}Co_{55.6}Sn_{116}$ by arc-melting a sample with starting composition $Sm_3Co_2Sn_3$. After the crystal structure was established (Table 2), the stoichiometric composition was used to prepare a single-phase sample. An X-ray powder diffraction pattern of the product obtained after arc melting agrees with the calculated one, although a small admixture cannot be ruled out due to the complicated nature of the diffraction pattern. Energy-dispersive X-ray (EDX) analysis of selected single crystals showed that the sample contains 39(1)% Sm, 20(1)% Co, and 41(1)% Sn, which is close to the composition obtained from the crystal structure refinement ($Sm_{117}Co_{55.6}Sn_{116} = Sm_{40.6}Co_{19.3}Sn_{40.2}$) and similar to the reported compositions of $Dy_{117}Co_{57}Sn_{112}$[19] and $Pr_{117}Co_{57}Sn_{112}$.[20] We note that no detailed analysis of the atomic arrangements and coordination polyhedra was performed for the latter compounds.

Table 2. Data collection and structure refinement parameters for $R_{117}Co_{52+\delta}Sn_{112+\gamma}$ (R = Sm, Tb).[a]

Composition	$Sm_{117}Co_{55.6(4)}Sn_{115.9(1)}$	$Tb_{117}Co_{58.8(7)}Sn_{111.2(8)}$
Space group	$Fm\bar{3}m$ (No. 225)	
a /Å	30.4156(5)	29.887(5)
V /Å^3	28138.7(8)	26696(8)
Z	4	
ρ_{calc} /g cm^{-3}	8.174	8.773
μ /mm^{-1}	37.189	44.220
Temperature /K	295	110
λ /Å	Mo-K_α, 0.71073	
$2\theta_{max}$ /°	65	56.4
Reflections collected	76979	95469
Unique reflections	2534	1674
Parameters refined	107	113
R_1, wR_2 [$F_o > 4\sigma(F_o)$]	0.028, 0.063	0.036, 0.077
Diff. peak and hole /e Å^{-3}	1.72 and –3.13	3.00 and –3.08
Goodness-of-fit	1.10	1.34

[a] Further details on the crystal structure investigations may be obtained from the Fachinformationszentrum Karlsruhe, 76344 Eggenstein-Leopoldshafen, Germany (fax: +49-7247-808-666; e-mail: crysdata@fiz-karlsruhe.de), on quoting the depository numbers CSD-422718 and -422719.

Single crystals of Tb- and Dy-containing analogues were selected from samples with the starting composition $R_3Co_2Sn_3$. The crystal structure refinements indicated that compositions of both phases differed from that of the Sm-containing phase in both Co and Sn content: $Tb_{117}Co_{59(1)}Sn_{111(1)}$ and $Dy_{117}Co_{58(1)}Sn_{111(1)}$. (The latter was also described previously by Salamakha et al.)[19] After establishing these compositions, attempts were made to synthesize single-phase materials. These efforts were unsuccessful, as arc-melted samples always contained an admixture of $R_3Co_4Sn_{13}$.

Crystal Structure Determination

The Sm-containing structure appears to be the most ordered among the three phases reported herein, and therefore we will focus on the crystal structure refinement and description of this compound. Due to the complexity of the structure, the occupancies of all positions were carefully examined in the course of refinement. All but one Sm positions appeared to be fully occupied. Atomic displacement parameters (ADPs) of the Sm atom at position 24*e* (x,0,0; $x \approx 0.34$) were substantially elongated in one direction. Thus, the refinement with two split positions (Sm61 and Sm62) was carried out. The sum of site occupancy factors (s.o.f.) for Sm61 and Sm62 was constrained to unity, while ADPs for these positions were set equal. A similar split model was applied to a Sn atom at position 32*f* (x,x,x; $x \approx 0.44$), resulting in Sn91 and Sn92.

The most complicated disorder is observed in the Co substructure. Only position Co1 is fully occupied, while all the other positions are split or mixed occupied:

(i) Two partially occupied positions, Co2 and Co6, are located inside a distorted trigonal prism of three Sm and three Sn atoms (Figure 1a and 1b). An analysis of the local disorder indicated physically impossible interatomic distances Co2′–Co2′′ and Co2′–Co6 (< 1.6 Å).[24] This suggested two possible atomic arrangements: either atoms Co2′ form a regular triangle with *d*(Co–Co) = 2.73 Å (Figure 1a) or atoms Co2′′ and Co6 form a flattened trigonal pyramid with *d*(Co–Co) = 2.41 Å (Figure 1b).

(ii) Position Co3 is coordinated by four Sn atoms and six Sm atoms. It is split into two positions, Co31 and Co32, along the Co3–Sn9 bond (Figure 1c). This disorder correlates with the aforementioned disorder of the Sn9 position to allow reasonable interatomic distances, *d*(Co31–Sn91) = 2.61 Å and *d*(Co32–Sn92) = 2.49 Å.

(iii) Refinement of position 32*f* (*x*,*x*,*x*; $x \approx 0.31$) as occupied solely by Co resulted in s.o.f. > 100%. Therefore, this position was refined as mixed occupied by Co and Sn atoms (Co41/Sn41). In the reported structures $Dy_{117}Co_{57}Sn_{112}$[19] and $Pr_{117}Co_{57}Sn_{112}$,[20] this position was refined as occupied only by Co atoms.

(iv) The most striking difference between the structure of $Sm_{117}Co_{55.6}Sn_{116}$ and those of $Dy_{117}Co_{57}Sn_{112}$ and $Pr_{117}Co_{57}Sn_{112}$ is the coordination of the Co5 atom. In the crystal structure of $Sm_{117}Co_{55.6}Sn_{116}$, this atom is shifted from the ideal position 4*b* (0.5,0.5,0.5) to position 24*e* (0.5,0.5,0.48) by 0.56 Å. Thus, each Co5 atom is disordered over six equivalent sites (s.o.f. = 1/6) that form an octahedron (Figure 1d).

(v) The Co5 atom is surrounded by eight Sn9 atoms at position 32*f* (*x*,*x*,*x*; $x \approx 0.44$) and six Co7 atoms at position 24*e* (0.5,0.5, ca. 0.57) (Figure 1d). Both positions are locally disordered, thus correlating with the disorder of the Co5 site. The total occupancy of Co71 and Co72 sites is 50%. The crystal structures of $Dy_{117}Co_{57}Sn_{112}$ and $Pr_{117}Co_{57}Sn_{112}$ do not contain positions analogous to Co71/Co72.

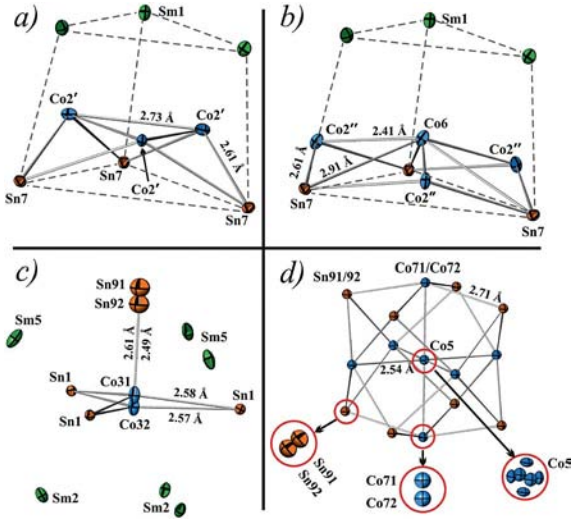

Figure 1. Local coordination environments of disordered Co atoms in the crystal structure of $Sm_{117}Co_{55.6}Sn_{116}$: (a) a regular triangle of the Co2′ sites within a trigonal prism of Sm1 and Sn7 atoms; (b) a flattened trigonal pyramid of the Co6 and Co2′′ sites within the same trigonal prism of Sm1 and Sn7 atoms; (c) the disorder of the Co3 and Sn9 sites along the Co3–Sn9 bond; (d) the correlated disorder of the Co5, Co7, and Sn9 sites.

Extensive disorder found in $Sm_{117}Co_{55.6}Sn_{116}$ is similar to those observed in Mg_2Al_3 and $NaCd_2$. The reciprocal lattice images of $Sm_{117}Co_{55.6}Sn_{116}$ also reveal the presence of diffuse scattering features (Figure S1), indicating possible superstructure formation that cannot be assessed by conventional X-ray crystallography.

The refinement of the crystal structures of $Tb_{117}Co_{59}Sn_{111}$ and $Dy_{117}Co_{58}Sn_{111}$ showed that they are similar to the crystal structure of $Sm_{117}Co_{55.6}Sn_{116}$. In the series, the size of the unit cell decreases from Sm to Tb to Dy, as expected from the lanthanide contraction; the unit cell parameters measured at 110 K were 30.293(3) (Sm), 29.887(5) (Tb), and 29.768(1) Å (Dy). While the Co sublattice appears to be similar in Sm- and Tb-containing structures, more disordered R and Sn positions were found for the latter compound. The R5 atom, which occupies a single site in $Sm_{117}Co_{55.6}Sn_{116}$, is split into three close-lying positions R51, R52, and R53, with a total occupancy of 100%. In turn, atoms Sn1, Sn3, and Sn8 that surround the disordered rare-earth sites are each split into two partially occupied positions. Note the increase in the Co/Sn ratio when going from the Sm-containing phase to the Tb-containing phase. This has two reasons: (i) the variation of the Co/Sn ratio at position M41; (ii) the partial occupancy of the split Sn91/Sn92 position in $Tb_{117}Co_{59}Sn_{111}$ vs. its full occupancy in $Sm_{117}Co_{55.6}Sn_{116}$.

Phase equilibria in the Sm–Co–Sn system at elevated temperatures have been studied recently,[25] and several intermetallic compounds have been found to form in this system: $SmCo_{1-x}Sn_2$ (x = 0.62), $Sm_{12}Co_6Sn$, Sm_6Co_2Sn, Sm_3CoSn_6, $Sm_3Co_8Sn_4$, $Sm_3Co_4Sn_{13}$, and $Sm_3Co_6Sn_5$. Surprisingly, only the latter compound has been structurally characterized thus far. The authors also mentioned the for-

Table 3. Ranges of bond lengths (in Å) in $Sm_{117}Co_{55.6}Sn_{116}$ and selected binary and ternary compounds.

Compound	Sm–Co	Sm–Sn	Sm–Sm	Co–Co	Co–Sn	Sn–Sn
$Sm_{117}Co_{55.6}Sn_{116}$	2.80–3.06	> 3.10	3.65–4.06	2.41–2.73	2.46–2.95	2.93
$Sm_3Co_6Sn_5$	3.00–3.24	3.16–3.18	3.93	2.56–2.69	2.58–2.92	3.10
$Dy_{117}Co_{52}Sn_{112}$	–	–	–	2.38–2.72	2.52–2.83	2.89
$R_xCo_ySn_z$[a]	–	–	–	2.40–2.68	2.47–2.83	> 2.81
Binaries[b]	2.79–3.19	> 3.10	> 3.14	2.37–2.73	2.62–2.74	> 2.84

[a] A summary of 40 entries found in the ICSD database for structurally characterized compounds in R–Co–Sn systems (R = La–Lu, but Sm). [b] A summary of bond lengths in CoSn, $CoSn_2$, Sm_2Co_{17}, $SmCo_2$, Sm_5Co_2, $SmCo_5$, $SmSn_3$, Sm_4Sn_3, and Sm_5Sn_3.

mation of a phase "Sm_2CoSn_2" with a large unit cell and its possible structural relationship to $Tb_{117}Fe_{52}Ge_{112}$. We believe that phase $Sm_{117}Co_{55.6}Sn_{116}$ reported by us herein represents the actual structure of "Sm_2CoSn_2".

A comparison of bond lengths in the crystal structure of $Sm_{117}Co_{55.6}Sn_{116}$ to those found in other related binary and ternary phases (Table 3) lends additional support to the correctness of the determined crystal structure. In the binary compounds and in $Sm_3Co_6Sn_5$, Sm–Co distances are typically shorter than Sm–Sn distances. The same situation is observed in $Sm_{117}Co_{55.6}Sn_{116}$, in which Sm–Co distances are shorter than Sm–Sn distances by approximately 0.2 Å. In turn, the shortest Sm–Sm distances in $Sm_{117}Co_{55.6}Sn_{116}$ (3.65 Å) are smaller than those in $Sm_3Co_6Sn_5$. This is not unusual, since even shorter Sm–Sm separations (3.14 Å) were reported in binary compounds. Co–Sn and Co–Co distances vary in a broad range 2.41–2.95 Å and are similar to those found in other ternary and binary structures. Sn–Sn distances are typically longer than 2.8 Å, which is also the case for $Sm_{117}Co_{55.6}Sn_{116}$. The interatomic distances for $Tb_{117}Co_{59}Sn_{111}$ also compare well to those observed in corresponding binary and ternary phases.

Topological Analysis of the Crystal Structure

The analysis of complicated crystal structures, with more than 1000 atoms in the unit cell, is not trivial. The original approach of Samson[1,2] implied identification of polyhedral building blocks (e.g. Friauf polyhedra in the structure of $NaCd_2$) and their fusion into more complicated fragments. This method has a disadvantage that not all atoms of the structure might be included into such polyhedra. Jones's description of complex intermetallics in terms of concentric polyhedra[11] and the related nested polyhedra approach developed by Parthé[10] provide the method for stepwise inclusion of all atoms in the polyhedra. These ideas have been employed successfully in recent works on the structures of complex intermetallics[26] and quasicrystal approximants.[12] They also will be used below to understand the structural organization of $Sm_{117}Co_{55.6}Sn_{116}$ and achieve a complete description of this complex structure. In the following analysis, all disordered atomic positions observed in the structure of $Sm_{117}Co_{55.6}Sn_{116}$ have been replaced with an idealized fully occupied site.

We first note the existence of three basic metal-centered polyhedra located at special positions of the face-centered cubic cell (Figure 2, top): (a) a 14-vertex $Co@Co_6Sn_8$ (magenta) at the edge centers and in the body center of the unit cell, (b) a 14-vertex $Sm@Co_8Sn_6$ (green) at the origin of the unit cell, and (c) a 22-vertex $Sm@Co_{12}Sn_{10}$ (blue) at the center of each octant. The arrangement of these polyhedra is identical to that of Al, Mn, and Cu atoms, respectively, in the crystal structure of Heusler alloy Cu_2MnAl.[27] We now proceed to examine how the rest of the structure emerges around these basic polyhedral units.

Polyhedron a, $Co@Co_6Sn_8$

The Co atom at the center of this polyhedron (Figure 3, top) is surrounded by an octahedron (OH) of Co atoms and

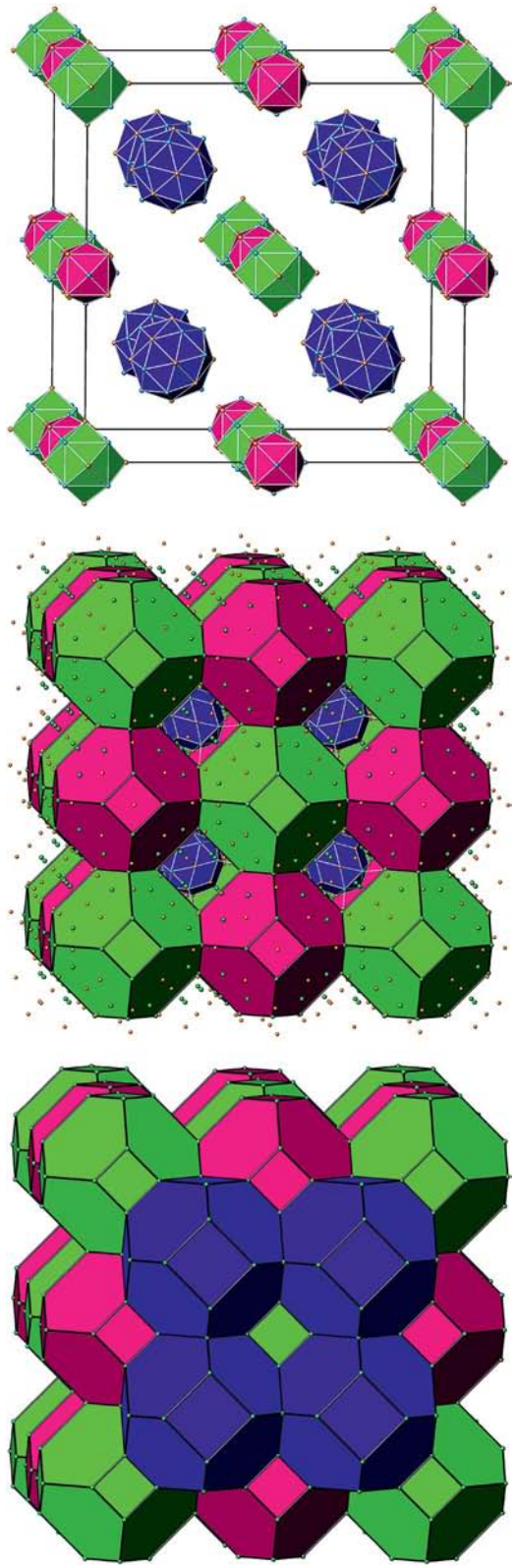

Figure 2. Polyhedral description of the crystal structure of $Sm_{117}Co_{55.6}Sn_{116}$. Top: basic polyhedral units *a* (magenta), *b* (green), and *c* (blue) are arranged in the Cu_2MnAl motif. Middle: large polyhedral units *A* (magenta) and *B* (green) form a face-centered cubic motif of NaCl, while the basic polyhedra *c* occupy the centers of all octants. Bottom: Concentric polyhedra *A*, *B*, and *C* (blue) include all atoms of the structure and share the outermost faces to form a void-free polyhedral arrangement.

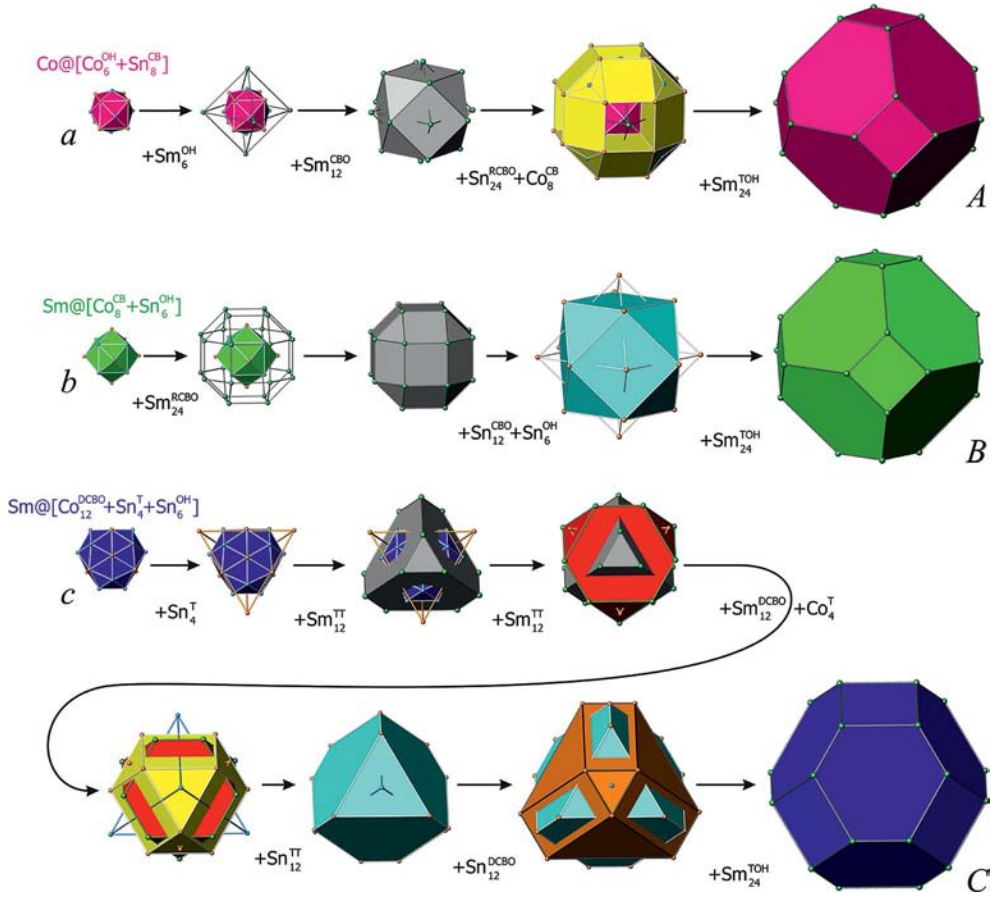

Figure 3. Nested polyhedra in the crystal structure of $Sm_{117}Co_{55.6}Sn_{116}$. The number of atoms appearing in each next polyhedral shell is given as a subscript, while their geometrical arrangement is represented with a superscript. See the text for further explanation.

a slightly more distant cube (CB) of Sn atoms. Further away is an octahedron (OH) of Sm atoms surrounded by a cuboctahedron (CBO) of 12 Sm atoms. This OH+CB+OH+CBO unit is surrounded by a shell consisting of 24 Sn atoms that form a rhombicuboctahedron (RCBO) and 8 Co atoms that center all triangular faces of the RCBO and form a cube (CB). The last shell is built of 24 Sm atoms forming a truncated octahedron (TOH).

The resulting large concentric polyhedral unit is labeled *A*. Its analysis clearly shows the separation of the polar intermetallic phase $Sm_{117}Co_{55.6}Sn_{116}$ into Sm-rich and Co/Sn-rich regions. We will see the same to be true for the other two polyhedral units discussed below.

Polyhedron b, $Sm@Co_8Sn_6$

In this polyhedron (Figure 3, middle), the central Sm atom is surrounded by a CB of Co atoms and an OH of Sn atoms. Note that now the order of the nearest polyhedra has changed relative to that observed in unit *a*, in order to conform to the shorter Sm–Co and longer Sm–Sn distances. Polyhedron *b* is surrounded by an RCBO made of 24 Sm atoms. The next shell is composed of 18 Sn atoms that form a CBO and an OH. Finally, a TOH of 24 Sm atoms completes this large polyhedral unit that is labeled *B*. Thus, the large concentric polyhedra *A* and *B* have a similar outer shape (TOH) and share their square faces to give an arrangement of the NaCl type (Figure 2, middle).

Polyhedron c, $Sm@Co_{12}Sn_{10}$

The basic polyhedra *c* (Figure 3, bottom) occupy the centers of all octants in the face-centered cubic motif formed by the *AB* polyhedra. As dictated by the structural arrangement, polyhedron *c* should have a tetrahedral local symmetry, which is in contrast to the octahedral symmetry of *a* and *b*. The central Sm atom is surrounded by a 22-atom shell consisting of 12 Co atoms that form a distorted cuboctahedron (DCBO) and 10 Sn atoms that form a tetrahedron (T) and an OH. Similar to the units *a* and *b*, the order of the nearest polyhedra conforms to the shorter Sm–Co and longer Sm–Sn distances. Polyhedron *c* is surrounded by an additional T of Sn atoms and then by 36 (12+12+12) Sm atoms forming three interpenetrating polyhedra: two TT (truncated tetrahedra) and one DCBO. The next shell is formed by a T of Co atoms and interpenetrating TT and DCBO of 24 (12+12) Sn atoms. Note that the interpenetrating polyhedra ($2Sm^{TT}+Sm^{DCBO}$ and $Sn^{TT}+Sn^{DCBO}$) are of the same atom type, which again shows the separation of the structure into regions of different polarity. Finally, a TOH of 24 Sm atoms completes the large concentric polyhedron *C* centered around the basic polyhedron ***c***.

The TOH *C* shares its six square faces with other *C* polyhedra and eight hexagonal faces with the truncated octahedra *A* and *B* (Figure 2, bottom). While *A* and *B* have similar shapes, with the hexagonal faces of the TOH more pronounced than the square ones, in *C* the areas of square and hexagonal faces become more comparable. The large polyhedra *A*, *B*, and *C* repeat the Cu_2MnAl-type arrangement of the basic small polyhedra *a*, *b*, and *c*.

Thus, the crystal structure of $Sm_{117}Co_{55.6}Sn_{116}$ can be described as a condensation of three convex multishell polyhedra, the outer structure of which is formed by a TOH of Sm atoms. Such polyhedral description results in the inclusion of all atoms of $Sm_{117}Co_{55.6}Sn_{116}$ in the concentric polyhedra and complete space filling. Moreover, the multishell approach clearly separates this polar intermetallic structure into Sm-rich and Co/Sn-rich regions. Such separation is also evident from an examination of radial distribution diagrams (Figure S2).

Magnetic Properties

The magnetic properties were studied on batches of single crystals (2–5 crystals in each sample; total weight ca. 0.5 mg). The identity of all selected crystals was confirmed by single-crystal X-ray diffraction to avoid interference from possible contamination.

$Sm_{117}Co_{55.6}Sn_{116}$ exhibits ferromagnetic ordering at 86(2) K (Figure 4a). The divergence of zero-field cooled (ZFC) and field cooled (FC) magnetization curves indicates some anisotropy of magnetic properties. A slight kink around 14 K might be due to a spin reorientation transition, although one cannot exclude the presence of a small amount of magnetic impurity on the surface of the crystals. Magnetic susceptibility (χ) at higher temperatures does not obey the Curie–Weiss law, which is typical of Sm-containing compounds.[28] The Sm^{3+} ion is characterized by low-lying excited states, which can be partially populated at higher temperatures, leading to nonlinearity of the $1/\chi$ vs. *T* dependence.

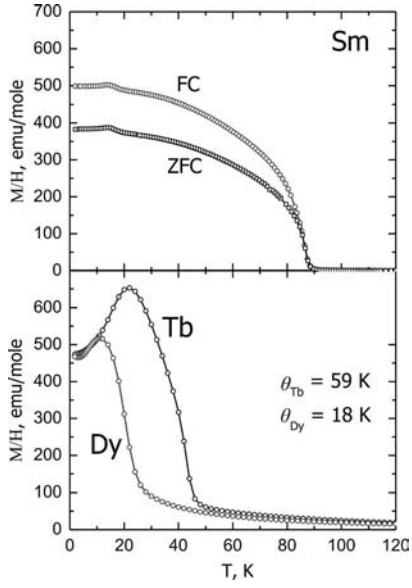

Figure 4. Temperature dependences of magnetization measured in an applied magnetic field of 100 G: (a) ZFC-FC curves for $Sm_{117}Co_{55.6}Sn_{116}$; (b) FC curves for $Tb_{117}Co_{59}Sn_{111}$ and $Dy_{117}Co_{59}Sn_{111}$.

Tb- and Dy-containing compounds exhibit more complicated magnetic behavior, clearly different from that of the Sm-containing analogue. The Curie–Weiss behavior is observed at higher temperatures, with positive Weiss constants of 59 and 18 K, respectively. This indicates that the nearest-neighbor coupling is ferromagnetic. The effective magnetic moments obtained from the Curie–Weiss fit (Figure S3) are 9.2 μ_B (Tb) and 10.4 μ_B (Dy) per rare-earth ion. These values are slightly smaller than the theoretically expected values of 9.7 μ_B (Tb) and 10.6 μ_B (Dy). Therefore, the Co sublattice is not magnetic in these compounds. Both compounds exhibit an abrupt increase in magnetic susceptibility at 38 and 20 K, respectively, followed by a maximum at 22 and 11 K, respectively, and a decrease at lower temperature (Figure 4b). This may indicate two consecutive magnetic phase transitions, a ferromagnetic ordering followed by an antiferromagnetic one. The maximum magnetic moments observed at 5 T and 1.8 K are significantly lower than the theoretically calculated values per rare-earth ion: 3.8 μ_B vs. 9.0 μ_B for Tb and 5.2 μ_B vs. 10 μ_B for Dy. Nevertheless, the observed values are still sufficiently high and do not exhibit saturation at the maximum applied field (Figure S4). This suggests that the magnetic ground states of $Tb_{117}Co_{59}Sn_{111}$ and $Dy_{117}Co_{58}Sn_{111}$ correspond to a canted antiferromagnet. Further studies are necessary to conclusively establish the type of magnetic ordering observed in these materials. In particular, the preparation of a Y-containing analogue will allow to verify whether the Co sublattice in these structures carries any magnetic moment, while the studies of isostructural germanides and stannides of other rare-earth metals will shed light on the peculiarities of magnetic exchange and ordering in this family of materials.

Conclusions

Giant unit cell compounds $Sm_{117}Co_{55.6}Sn_{116}$, $Tb_{117}Co_{59}Sn_{111}$, and $Dy_{117}Co_{58}Sn_{111}$ crystallize in the $Tb_{117}Fe_{52}Sn_{112}$ structure type. Their crystal structure can be understood by identifying three multishell polyhedral clusters arranged in the manner analogous to the arrangement of atoms in the structure of Heusler alloy Cu_2MnAl. The outer shell of each cluster is a truncated octahedron composed of 24 Sm atoms, while the inner shells have a number of polyhedral shapes, the symmetry of which is dictated by the local symmetry of the site at the center of the multishell cluster. Importantly, each individual shell is built of either Sm atoms or Co/Sn atoms, thus emphasizing the polar nature of these intermetallics. $Sm_{117}Co_{55.6}Sn_{116}$ exhibits ferromagnetic ordering of Sm magnetic moments at 86 K, while both $Tb_{117}Co_{59}Sn_{111}$ and $Dy_{117}Co_{58}Sn_{111}$ appear to undergo two consecutive phase transitions below 50 K, from the paramagnetic to the ferromagnetic to the canted antiferromag-

netic state. The evaluation of the magnetic moments carried by the Tb and Dy sites suggests that the Co sublattice in these structures is nonmagnetic.

Experimental Section

Synthesis: Bars of Sm, Tb, and Dy (Michigan Chem. Corp., all 99.9%) were finely dispersed by using stainless steel files. Tin shots (Alfa Aesar, 99.99%) were used as received. Cobalt powder (Alfa Aesar, 99.5%) was additionally purified by heating under a flow of H_2 gas at 775 K for 5 h. All manipulations during sample preparation were carried out in an Ar-filled dry box (content of O_2 < 1 ppm). The starting materials were mixed together, pressed into pellets (total mass 0.25 g), and arc melted. The pellets were carefully remelted 5–6 times to achieve homogeneity. The obtained ingots were crushed, and single crystals were selected for structural analysis and investigation of magnetic properties. To improve the homogeneity of the Sm-containing sample, one arc-melted ingot was placed into a silica tube, sealed under vacuum ($< 10^{-2}$ mbar), and annealed at 1025 K for five days. An analysis of the single crystals selected from the annealed sample revealed a disorder similar to that observed for the crystals selected from samples immediately after arc melting.

Physical Measurements: Powder X-ray diffraction was performed with a Rigaku DMAX 300 Ultima III diffractometer (Cu-K_a, λ = 1.54185 Å). Elemental analysis of selected single crystals was carried out with a JEOL 5900 scanning electron microscope with an EDX attachment. Metallic Sn and Co, as well as SmF_3, were used as internal standards. Magnetic measurements were performed on batches of selected single crystals with a Quantum Design SQUID MPMS-XL magnetometer. DC magnetic susceptibility measurements were carried out in an applied field of 0.01 T in the 1.8–300 K temperature range. Field-dependent magnetization was measured at 1.8 K with an applied magnetic field varying from 0 to 5 T.

Single-Crystal X-ray Diffraction: A single crystal of $Sm_{117}Co_{55.6}Sn_{116}$ was glued with epoxy cement on the tip of a quartz fiber and mounted on a goniometer head of a Bruker AXS SMART diffractometer with an APEX-II CCD detector. A 295 K dataset was recorded as ω-scans at 0.3° step width and integrated with the Bruker SAINT software package.[29] The dataset was indexed in a face-centered cubic unit cell. An analysis of intensity statistics showed the space group to be $Fm\bar{3}m$. The absorption correction was based on fitting a function to the empirical transmission surface as sampled by multiple equivalent measurements (SADABS).[30] Solution and refinement of the crystal structure was carried out by using the SHELX suite of programs.[31] The structure was solved in the $Fm\bar{3}m$ space group (No. 225). Most of the heavy atom positions (Sm and Sn) were located with direct methods, while the other atomic positions were located from a combination of least-squares refinements and difference Fourier maps. The final refinement was performed with anisotropic atomic displacement parameters for all atoms. Further details of the crystal structure determination can be found in the "Results and Discussion" section. A summary of pertinent information related to unit cell parameters, data collection, and refinements is provided in Table 2.

After establishing the crystal structure of $Sm_{117}Co_{55.6}Sn_{116}$, the dataset for the Tb-containing analogue was collected at 110 K to reduce the atomic thermal motion. The crystal was suspended in Paratone-N oil (Hampton Research) and mounted on a cryoloop, which was placed in an N_2 cold stream, cooled down at 5 K/min, and allowed to equilibrate at 110 K for one hour prior to data collection. The data processing and crystal structure analysis followed the routine described above for $Sm_{117}Co_{55.6}Sn_{116}$.

Supporting Information (see footnote on the first page of this article): Reciprocal space images, the radial distribution diagram, additional magnetic plots.

Acknowledgments

This research is supported by the National Science Foundation CAREER Award (DMR-0955353).

[1] a) S. Samson, *Nature* **1962**, *195*, 259–262; b) Q.-B. Yang, S. Andersson, L. Stenberg, *Acta Crystallogr., Sect. B* **1987**, *43*, 14–16.
[2] S. Samson, *Acta Crystallogr.* **1965**, *19*, 401–413.
[3] M. L. Fornasini, B. Chabot, E. Parthé, *Acta Crystallogr., Sect. B* **1978**, *34*, 2093–2099.
[4] S. Samson, *Acta Crystallogr.* **1967**, *23*, 586–600.
[5] G. Cordier, V. Müller, *Z. Kristallogr.* **1993**, *205*, 353–354.
[6] a) M. H. Booth, J. K. Brandon, R. Y. Brizard, C. Chieh, W. B. Pearson, *Acta Crystallogr., Sect. B* **1977**, *33*, 30–36; b) S. Thimmaiah, G. J. Miller, *Chem. Eur. J.* **2010**, *16*, 5461–5471.
[7] a) T. Weber, J. Dshemuchadse, M. Kobas, M. Conrad, B. Harbrecht, W. Steurer, *Acta Crystallogr., Sect. B* **2009**, *65*, 308–317; b) M. Conrad, B. Harbrecht, T. Weber, D. Y. Jung, W. Steurer, *Acta Crystallogr., Sect. B* **2009**, *65*, 318–325.
[8] J.-M. Dubois, E. Belin-Ferré (Eds.), *Complex Metallic Alloys: Fundamentals and Applications*, Wiley-VCH, Weinheim, **2010**.
[9] M. Feuerbacher, C. Thomas, J. P. A. Makongo, S. Hoffmann, W. Carrillo-Cabrera, R. Cardoso, Yu. Grin, G. Kreiner, J.-M. Joubert, T. Schenk, J. Gastaldi, H. Nguyen-Thi, N. Mangelinck-Noël, B. Billia, P. Donnadieu, A. Czyrska-Filemonowicz, A. Zielinska-Lipiec, B. Dubiel, T. Weber, P. Schaub, G. Krauss, V. Gramlich, J. Christensen, S. Lidin, D. Fredrickson, M. Mihalkovic, W. Sikora, J. Malinowski, S. Brühne, T. Proffen, W. Assmus, M. de Boissieu, F. Bley, J.-L. Chemin, J. Schreuer, W. Steurer, *Z. Kristallogr.* **2007**, *222*, 259–288.
[10] B. Chabot, K. Cenzual, E. Parthé, *Acta Crystallogr., Sect. A* **1981**, *37*, 6–11.
[11] A. J. Bradley, P. Jones, *J. Inst. Met.* **1933**, *51*, 131–157.
[12] Q. Lin, J. D. Corbett, *Struct. Bonding (Berlin)* **2009**, *13*, 1–39, and references therein.
[13] a) F. C. Frank, J. S. Kasper, *Acta Crystallogr.* **1958**, *11*, 184–190; b) F. C. Frank, J. S. Kasper, *Acta Crystallogr.* **1959**, *12*, 483–499.
[14] D. C. Fredrickson, S. Lee, R. Hoffmann, *Angew. Chem.* **2007**, *119*, 2004; *Angew. Chem. Int. Ed.* **2007**, *46*, 1958–1976.
[15] V. Smetana, V. Babizhetskyy, G. V. Vajenine, A. Simon, *Angew. Chem.* **2006**, *118*, 6197; *Angew. Chem. Int. Ed.* **2006**, *45*, 6051–6053.
[16] C. Hoch, M. Wendorff, C. Röhr, *Z. Anorg. Allg. Chem.* **2003**, *629*, 2391–2397.
[17] V. K. Pecharsky, O. I. Bodak, V. K. Bel'skii, P. K. Starodub, I. R. Mokra, E. I. Gladyshevskii, *Kristallografiya* **1987**, *32*, 334–338.
[18] W. He, J. Zhang, L. Zeng, *Powder Diffr.* **2007**, *22*, 312–315.
[19] P. Salamakha, O. L. Sologub, G. Bocelli, S. Otani, T. Takabatake, *J. Alloys Compd.* **2001**, *314*, 177–180.
[20] W. He, J. Zhang, J. Yan, Y. Fu, L. Zeng, *J. Alloys Compd.* **2010**, *491*, 49–52.
[21] W. Harms, Dissertation Universitaet Freiburg/Breisgau, **2008**.
[22] V. Smetana, V. Babizhetskyy, C. Hoch, A. Simon, *J. Solid State Chem.* **2007**, *180*, 3302–3309.
[23] M. Tillard-Charbonnel, N. Chouaibi, C. Belin, J. Lapasset, *Eur. J. Solid State, Inorg. Chem.* **1992**, *29*, 347–359
[24] The prime symbol is used to indicate symmetrically equivalent positions, e.g. Co2, Co2′, and Co2′′.

[25] L. Romaka, V. V. Romaka, M. Konyk, N. Melnychenko-Koblyuk, *Chem. Met. Alloys* **2008**, *1*, 198–203.
[26] a) V. Ya. Shevchenko, V. A. Blatov, G. D. Ilyushin, *Struct. Chem.* **2009**, *20*, 975–982; b) V. A. Blatov, G. D. Ilyushin, D. M. Proserpio, *Inorg. Chem.* **2010**, *49*, 1811–1818.
[27] O. Heusler, *Ann. Phys.* **1934**, *19*, 155–201.
[28] R. L. Carlin, *Magnetochemistry*, Springer-Verlag, Berlin, **1986**.
[29] *SMART and SAINT*, Bruker AXS Inc., Madison, WI, USA, **2007**.
[30] G. M. Sheldrick, *SADABS*, University of Göttingen, Göttingen, Germany, **1996**.
[31] G. M. Sheldrick, *Acta Crystallogr., Sect. A* **2008**, *64*, 112–122.
Received: February 27, 2011
Published Online: May 24, 2011

